Coding two-dimensional images with orbital angular momentum of light

JIAQI CHU,[1] XUEFENG LI,[1] QUINN SMITHWICK,[2] DAPING CHU[1,*]

[1]*P&S Group, Engineering Department, University of Cambridge*
[2]*Disney Research*
**Corresponding author: dpc31@cam.ac.uk*

We consider decoding of two-dimensional information encoded with orbital angular momentum (OAM) of light. Spiral phase plates and spatial light modulators are used to prepare encoding and decoding OAM states, respectively. We show that with selective coding OAM states, off-axis points and spatial variables encoded with OAM are reproducible.

OCIS codes: *(050.1970) Diffractive optics; (080.4865) Optical vortices; (070.6120) Spatial light modulators.*

Light may carry spin angular momentum and orbital angular momentum (OAM) [1]. Spin angular momentum is associated with circular polarization of light, and OAM is a property of light related to the phase distribution of the optical wave front. Unlike spin angular momentum (i.e. polarization), which has only two orthogonal modes, OAM has theoretically an infinite number of orthogonal modes.

Beams having helical phase fronts described by $e^{il\phi}$, where l can be an integer or fraction and ϕ is the angular coordinate, have been shown to possess well-defined OAM of $l\hbar$ per photon [2,3]. The theoretically unbounded state space provided by OAM beams enables enhanced free-space and fiber communications [4-8]. Methods ranging from diffractive optics [9,10], spiral phase plates [11], and mode converters [2,12], to q-plates [13,14] are used to generate OAM beams. In general, bits of data are either encoded as OAM states of the beam [8] or carried by the amplitude of the on-axis point of the OAM beam [5], then decoded from a multiplexed beam. OAM mode-division multiplexing is used in combination with other multiplexing schemes to achieve additional degrees of freedom [15] and increase channel capacity. While coding one-dimensional information in OAM modes has been demonstrated, coding two-dimensional information has not been studied.

In this paper, we describe the use of OAM beams in coding two-dimensional patterns. In an attempt to code an image with OAM, we decompose the image into an on-axis point and off-axis points. Fig. 1(a) sketches coding of an off-axis point with OAM. Assume x and y are two independent variables of the cardinal coordinate, ϕ is the azimuthal angle in the polar coordinate, and l_1 and l_2 represents two states of OAM, we denote an off-axis point with amplitude a and phase φ as

$$g(x,y) = a\delta(x-x_0, y-y_0)e^{i\varphi}. \tag{1}$$

As the off-axis point is encoded and decoded with OAM states l_1 and l_2, respectively, the resultant far field is found to be

$$G(f_X, f_Y) = \mathcal{F}\left\{g(x,y)e^{il_1\phi}e^{il_2\phi}\right\}, \tag{2}$$

where f_X and f_Y are two independent variables of the cardinal coordinate after the Fourier transform. Working together, the encoding and decoding of the OAM state modulates the point with the updated spiral phase characterized by $e^{il\phi(x,y)}$, where $l=l_1+l_2$.

When $l=0$, the decoding OAM state cancels the encoding OAM state, and the far field contains Fourier information of the original point in that

$$\begin{aligned} G(f_X, f_Y) &= \mathcal{F}\left\{g(x,y)\right\} \\ &= ae^{i\varphi}e^{-i2\pi(f_X x_0 + f_Y y_0)}. \end{aligned} \tag{3}$$

When $l\neq 0$, the decoding OAM state does not match the encoding state. Following the convolution theorem, the far field can be found by

$$\begin{aligned} G(f_X, f_Y) &= \mathcal{F}\left\{g(x,y)\right\} \otimes \mathcal{F}\left\{e^{il\phi}\right\} \\ &= ae^{i\varphi}e^{-i2\pi(f_X x_0 + f_Y y_0)} \otimes \mathcal{F}\left\{e^{il\phi}\right\}. \end{aligned} \tag{4}$$

We define $\mathcal{Z}_l(x) = \int_0^x tJ_l(t)dt$, where the function J_l is the l th-order Bessel function of the first kind. The Fourier transform of spiral phase is then given by

$$\mathcal{F}\left\{e^{il\phi}\right\} = \frac{1}{(2\pi r)^2}(-i)^l \mathcal{Z}_l(2\pi\rho_0 r)e^{il\theta}, \tag{5}$$

where (r,θ) is the polar coordinate in the (f_X, f_Y) plane, and ρ_0 is radius of the spiral phase affected. Eq. (5) describes a kernel with circular symmetry, with the amplitude of a circular central region close to 0. Calculated amplitude profile and radial intensity are sketched in Fig. 1 (b) and (c), respectively. We find radius r_0 of the central dark region at $1/e^2$ of the maximum intensity. Since the spectrum of a delta function extends uniformly over the entire frequency domain, encoding and decoding of a single point with unmatched encoding and decoding OAM states results in a centered dark region.

Contributed by the on-axis point and all the off-axis points, information of a two-dimensional pattern can be preserved by encoding and decoding with matched OAM modes. For patterns

encoded and decoded using unmatched OAM states, the resultant far field contains a hole, which is spatially separable from useful information decoded with a matched OAM state.

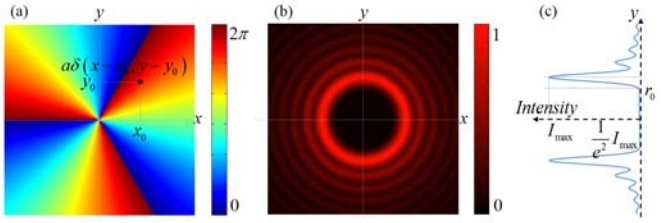

Fig. 1. (a) Sketch of an off-axis point modulated by an OAM state. (b) Normalized amplitude of Eq. (3) when the charge $l=3$. The amplitude profile is calculated by evaluating the integral in terms of weighted sums of Bessel functions and Struve functions. (c) Calculated radial intensity.

In a multiplexed beam, multiple two-dimensional patterns are coded with a series of OAM states

$$A(x,y)=\sum_m A_m(x,y)e^{il_m\phi}. \tag{6}$$

Decoded by a spiral phase $e^{il_0\phi}$ corresponding to a selected OAM state, the far field can be expressed as

$$G(f_X,f_Y)=\mathcal{F}\left\{\sum_m A_m(x,y)e^{i(l_m+l_0)\phi}\right\}. \tag{7}$$

Due to linearity of the Fourier transform, the far field after encoding, multiplexing and decoding is given by

$$\begin{aligned} G(f_X,f_Y)&=\sum_m \mathcal{F}\left\{A_m(x,y)e^{i(l_m+l_0)\phi}\right\} \\ &=\mathcal{F}\left\{A_k(x,y)\right\}+\sum_{m,m\neq k}\mathcal{F}\left\{A_m(x,y)e^{i(l_m+l_0)\phi}\right\}. \end{aligned} \tag{8}$$

Decoded by a selected OAM state l_0, only the pattern encoded with the matched state l_k=-l_0 is preserved, while the energy of the other unmatched states are shifted outwards. Therefore Fourier information of $A_0(x,y)$ is extracted after OAM modulation.

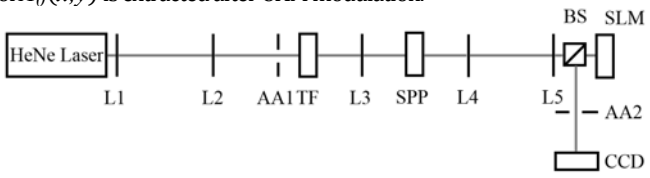

Fig. 2. Schematic overview of encoding and decoding a two-dimensional image with OAM, where L1 to L5 are the lenses, AA1 and AA2 are the adjustable apertures, TF is the transparency film, SPP is the spiral phase plate, BS is the beam splitter, and SLM is the spatial light modulator.

We experimentally demonstrate coding one image with an OAM state. A sketch of the optical system is shown in Fig. 2. Light emitted from a 632.8 nm HeNe laser is expanded by two lenses (L1 and L2) and illuminated on a removable transparency film (TF) which imprints a two-dimensional image onto the projected beam. An adjustable aperture (AA1) is placed in front of the transparency film to remove the noisy outer portion of the expanded beam. A lens (L3) is inserted after the transparency film to adjust projection distance of the image. Information containing the image is incident on a spiral phase plate (SPP) with an $e^{il_0\phi}$ phase distribution, encoding the transformed image into an OAM mode l_0. For decoding, the encoded pattern is relayed onto a phase-only LCoS spatial light modulator (SLM) using two lenses (L4 and L5). A second adjustable aperture (AA2) is used to filter out everything but the first diffraction order. Output of the system is captured using a CCD camera. We use a beam splitter (BS) to ensure perpendicular incidence on the SLM.

As derived above, the pattern at the first diffraction order depends on the sum of the encoding and decoding OAM states. Without the transparency film, we expect to see either a bright or a dark region in center, depending on whether the decoding OAM state cancels the encoding one so that the sum equals zero. With the transparency film's image coded in the beam, we expect to see projection of the pattern on the CCD camera when the decoding OAM state matches the encoding OAM state. For unmatched encoding and decoding OAM states, we expect to obtain a convolution of the encoded pattern and the kernel with a dark region in center.

In our experiment, we generate the encoding OAM states by the use of spiral phase plates. The SLM displays a forked diffraction grating (i.e. a spiral phase distribution with a blazed linear grating) with adjustable charge to create different decoding OAM states at the first diffraction order. The blazed grating is used to separate out the zero order from the first order.

Fig. 3(a) shows observed intensity profiles in the case that no image is coded. When the encoding spiral phase plate is removed and the SLM just displays a blazed grating (no spiral decoding phase) , the first diffraction order of the output is recorded as a reference. With an encoding spiral phase plate and decoding SLM forked diffraction grating, when the sum of the OAM states equals 0, a bright intensity occurs in the center. Acting as an updated OAM state, a centered dark region occurs when the decoding OAM state does not cancel the encoding OAM state. The radius increases with the absolute value of sum of the coding (encoding and decoding) OAM states.

Fig. 3(b) shows observed intensity profiles in the case that two-dimensional information on a transparency film is coded with OAM. Without encoding or decoding OAM states, the reference is just the projection of the transparency film diffracted by the SLM's blazed grating. We then encode the two-dimensional pattern on the transparency film with OAM state l_0=-4 prepared by a spiral phase plate. Compared to the reference, we are able to decode the two-dimensional image using the SLM to display a phase dislocation with charge l_k=+4. As the absolute value of the sum of the encoding and decoding OAM states increases, a dark region gradually appears in center of the image, with some features of the projected image surrounding the hole. As the absolute value reaches a large enough magnitude, the central region becomes large enough so that the size of the dark region is larger than that of the decoded two-dimensional image. When the decoded image and the circular pattern are mapped together, they are spatially separable, which indicates that information coded with unmatched OAM states has no impact on the information coded with matched OAM states, considering only the central region, even if they are mapped and mode-multiplexed into a beam bundle. In Fig. 3(b), we encoded a bold Arial character 'A' with a height of 5mm. The size of dark region reaches sufficiently large size when the absolute value of the sum exceeds 30.

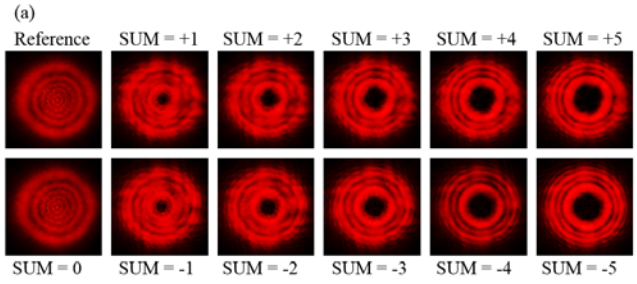

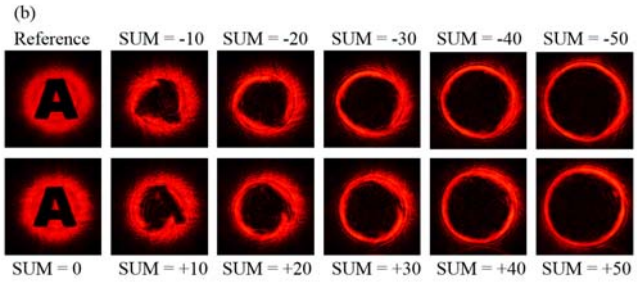

Fig. 3 (a) Observed intensity profiles at the first diffraction order when no image is coded and (b) observed intensity profiles at the first diffraction order for a range of decoding OAM states when a two-dimensional pattern is coded. The encoding OAM state prepared by the spiral phase plate is -4.

In order to show that our setup can code larger images, we create a range of encoding and decoding OAM states with specific beam waists. The radius of the central dark region of the light encoded by the OAM states l_0=-4 and decoded by a set of sequential OAM states is studied (Fig. 4). The trend of the calculated radii agrees well with experimental results in that the size of the dark region increases with the sum of encoding and decoding OAM states, which means a larger sum allows coding of larger images to be separated from unwanted rings. However, generation of OAM beams with larger l values is more problematic in that they require higher resolutions of spiral phase. Though the state space provided by OAM is theoretically infinite, the trade-off between image size and coding states would set limits to decoding images from multiplexed OAM beam.

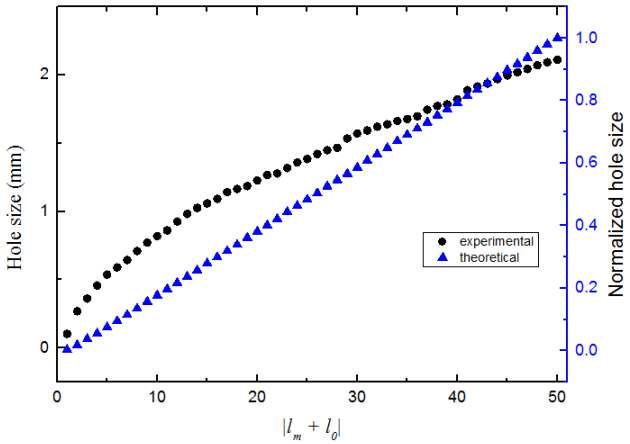

Fig. 4 Modelled and measured radius of the central dark region with respect to absolute value of sum of the encoding and decoding OAM states.

In addition to the radius of dark regions provided by different OAM states, we characterise the energy distribution of outside rings present using different beam waists of the incident light. Intensity of part of a generated ring is summed along one axis and derivative of energy with respect to the axis is calculated. Fig. 5 indicates that the energy distribution of an outside ring is symmetrical with respect to the radial direction. Moreover, the derivative of energy reaches highest at the same position for all beam waists, which confirms that the radial positions of highest intensity of the rings are stationary. After the derivatives are maximal, they decrease proportionally with the radial distance, which indicates that the radius of dark regions for different beam waists can be found at the same radial positions, as well. Therefore, selection of the coding OAM states is less relevant with the exact patterns to be coded.

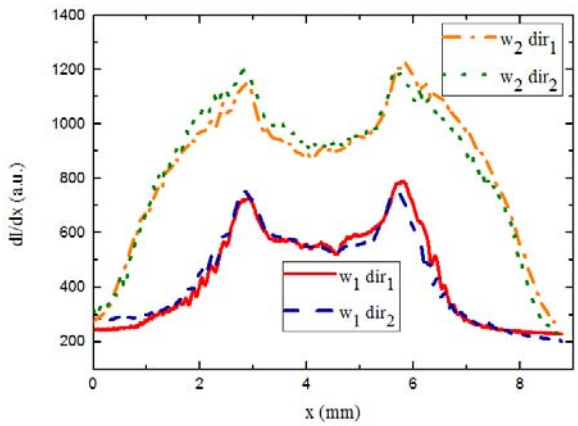

Fig. 5 Derivative of energy with respect to two directions.

Thickness of the phase-only LCoS SLM used to create the decoding mode varies across the surface (Fig. 6(a)), which contributes to phase departure of the decoding spiral phase. In the central 5mm area where the light is incident on, thickness varies from 2.644 to 2.2538 microns. In order to investigate its effect, the distortion introduced by thickness variation of the LCoS device across the surface is calculated. For calibration of the LCoS, the beam without OAM modulation and coding images is incident in centre of the surface, where a binary grating is displayed. Within the area of the calibration beam, dependency of phase modulation of the LCoS on loaded grey scale pattern is averaged. However, in practice the positions where the thickness of the LCoS surface is thicker than average modulate phase more than intended, and the thinner positions modulate less. The phase departure considering thickness variation is calculated. From Fig. 6(b) we can see that 0.2π phase departure results in unevenness and also blur edges of the image. This may explain one of the reasons leading to imperfections of the regenerated image shown in Fig. 3 (b).

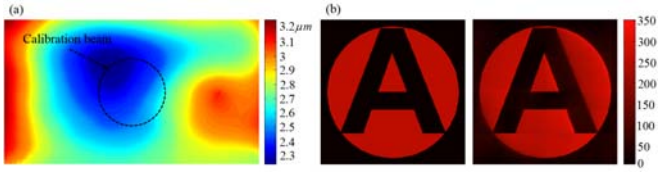

Fig. 6 (a) Thickness distribution of the LCoS SLM. (b) Ideal amplitude and calculated distorted amplitude due to phase departure introduced by thickness variation of the LCoS SLM.

In conclusion, we present the concept of coding two-dimensional images with OAM, and we demonstrate that it works by spatially separating the reconstructed image and unwanted rings. We also analyze ring size of over 50 updated OAM states and indicate that larger patterns can be coded. We believe that this principle can be used in high-dimension optical communication and imaging techniques based on OAM states.

Acknowledgment. This research was performed under a joint collaboration between Disney Research and the University of Cambridge through the CAPE consortium.

References

1. L. Allen, M. J. Padgett, and M. Babiker, in *Progress in Optics* XXXIX (Elsevier Science Publishers B. V., 1999), p. 294.
2. L. Allen, M. W. Beijersbergen, R. J. C. Spreeuw, and J. P. Woerdman, Phys. Rev. A **45**, 8185 (1992).
3. S. S. R. Oemrawsingh, X. Ma, D. Voigt, A. Aiello, E. R. Eliel, and J. P. Woerdman, Phys. Rev. Lett. **95**(24), 240501 (2005).
4. G. Gibson, J. Courtial, M. J. Padgett, M. Vasnetsov, V. Pas'ko, S. M. Barnett, and S. Franke-Arnold, Opt. Express **12**, 5448 (2004).

5. J. Wang, J. Y. Yang, I. M. Fazal, N. Ahmed, Y. Yan, H. Huang, Y. Ren, Y. Yue, S. Dolinar, M. Tur and A. E. Willner, Adv. Opt. Photone. **5**, 456(2013).
6. N. Bozinovic, Y. Yue, Y. Ren, M. Tur, P. Kristensen, H. Huang, A. E. Willner, S. Ramachandran, Science **340**(6140), 1545 (2013).
7. B.I. Djordjevic, Opt. Express **19**(15), 14277 (2011).
8. M. Krenn, R. Fickler, M. Fink, J. Handsteiner, M. Malik, T. Scheidl, R. Ursin, and A. Zeilinger, New. J. Phys. **16**(11), 113028 (2014).
9. M. Mirhosseini, O. S. Magana-Loaiza, C. Chen, B. Rodenburg, M. Malik, and R. W. Boyd, Opt. Express **21**(25), 30196 (2013).
10. G. C. G. Berkhout, M. P. J. Lavery, J. Courtial, M. W. Beijersbergen, and M. J. Padgett, Phys. Rev. Lett. **105**(15), 153601 (2010).
11. K. Sueda, G. Miyaji, N. Miyanaga, and M. Nakatsuka, Opt. Express **12**, 3548 (2004).
12. J. Coutial, M. J. Padgett, Opt. Commun. **159**(1), 13 (1999).
13. L. Marrucci, C. Manzo, and D. Paparo, Opt. Commun. **96**(16), 163905 (1993).
14. L. Marrucci, J. Nanophoton. **7**(1), 078598 (2013).
15. G. Molina-Terriza, J. P. Torres, and L. Torner, Nature Phys. **3**(5), 305 (2007).